J. Biophotonics **10**, 1421–1429 (2017) / **DOI** 10.1002/jbio.201600194

Journal of BIOPHOTONICS

FULL ARTICLE

Tail artifact removal in OCT angiography images of rodent cortex

Utku Baran[1, 2], *Woo June Choi*[1], *Yuandong Li*[1], *and Ruikang K. Wang*[*, 1]

[1] Department of Bioengineering, University of Washington, Seattle, WA, USA
[2] Department of Electrical Engineering, University of Washington, Seattle, WA, USA

Received 5 July 2016, revised 16 August 2016, accepted 21 August 2016
Published online 8 September 2016

Key words: optical coherence tomography, OCT angiography, artifact removal, stroke

Optical coherence tomography angiography (OCTA) is a surging non-invasive, label-free, in vivo volumetric imaging method, currently being translated to clinical ophthalmology and becoming popular in neuroscience. Despite its attractiveness, there is an inherent issue of using OCT angiograms for quantitative cerebrovascular studies: The dynamic scattering of moving erythrocytes within pial vasculature creates tail-like artifacts that shadow the capillary vessels in the deeper layers of cortex. This false flow effect is relatively benign for qualitative visualization purposes, but it might have a significant impact on quantitative interpretation of angiographic results. In this work, we propose a simple image processing method to remove these tail artifacts in depth-resolved OCTA images using an adaptive enface mask generated with OCT structural images. We demonstrate the effectiveness of our method by comparing vessel densities and vessel similarities of depth-resolved OCT angiograms in a stroke study in a rodent model, *in vivo*. Thanks to the ability of seeing through the tails of pial vessels, capillary vessels beneath these vessels could be recovered to some extend in the deeper layers of mouse cerebral cortex, leading to a more accurate quantification.

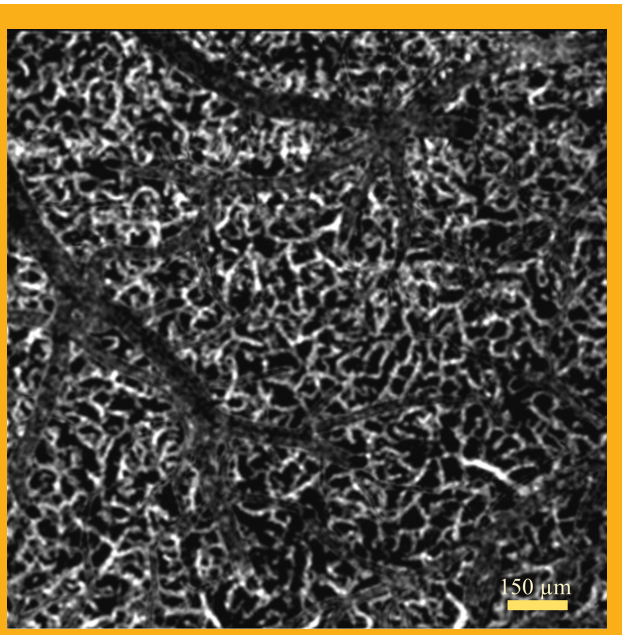

Tail artifact removed enface OCT angiogram of deeper layer *in vivo* mouse cortex.

1. Introduction

Traditionally, histological analysis has been used to study microvascular networks [1], which is totally invasive and may not well represent the vascular morphology *in vivo*. Popular non-invasive label-free imaging techniques, such as laser speckle contrast imaging [2], Doppler ultrasound [3], and functional magnetic resonance imaging [4] also have been used to study microvascular changes in many physiological states. However, the limited spatial and/or temporal resolution prevent these techniques from imaging

* Corresponding author: e-mail: wangrk@uw.edu

small blood vessels such as capillaries. On the other hand, two-photon microscopy [5] allows high-resolution imaging of neural and microvascular activities in rodent models, but it is usually limited with speed, field of view, penetration depth, and the necessity of contrasting agents.

Optical coherence tomography (OCT), a well-established technique in biomedical imaging, enables volumetric morphological visualization of tissue microstructures *in vivo* with a micrometer-scale image resolution [6]. OCT angiography (OCTA), a popular extension of OCT, is able to image blood perfusion in the functional vessels down to capillary level, *in vivo* [7, 8]. Recent studies have validated the accuracy of OCTA for in vivo blood flow imaging with multi-photon microscopy on a mouse cerebrovascular model [9] and with laser speckle contrast imaging on a human skin microvascular model [10]. OCTA has been used to study the microvasculature of a variety of tissues *in vivo*, including healthy and diseased human skin [11], human retina [12], and mouse cerebral microvasculature [13].

Although OCTA is an attractive volumetric microvascular imaging method, 3D visualization of microvasculature is typically difficult to interpret, which in part drives most researchers to use enface maximum intensity projection (MIP) images of OCTA for their studies. It is mostly because of the tail-like artifacts that appear in the deeper layers coming from the strong scattering property of erythrocytes within overlying vasculature. Such tails appear as elongated vessels in the axial direction and cause overlap between superficial and deep layers [14]. Since signal strength of the tail artifact is usually much stronger or comparable to the scattered signals at the deep vessels, the flow signals of capillaries in the cortex subsequent to the pial vessels are overlapped or hidden by the tail artifacts. This adverse effect is relatively benign for the visualization of overall vessel network from the OCT angiogram. However, it has a significant impact on quantitative interpretation of angiographic results.

A few post-processing methods have been proposed to tackle this problem in the field of ophthalmic imaging. The most of these methods rely on a slab-subtraction algorithm. In these methods, the vascular pattern of superficial microvasculature is subtracted from an enface MIP image of a deeper layer [15, 16]. Unfortunately, this method replaces the tail artifact with a shadow cast (area with absence of blood vessels), leaving apparent gaps within microvascular plexus that are difficult to reconstruct.

In another work, Zhang et al. developed a projection-resolved OCTA algorithm to improve the shadow cast problem that occurs when using the previous tail artifact removal methods [17]. This method can identify multiple vessels along an A-line of OCTA image for ophthalmology applications after effectively suppressing the projection artifacts on both enface and cross-sectional angiograms. Briefly, this algorithm first detects the peaks in the A-lines of OCTA, upon which to keep the decorrelation values at the successive peak positions (vessels), and then set the rest to zero. One drawback of this method is that it heavily relies on an accurate peak detection. For ophthalmology applications, this may be a reasonable requirement where: 1) Most of the vessels in retinal layers have similar diameters so that the peaks are relatively easier to detect in an A-line, and 2) Retinal tissue is relatively transparent. However, this algorithm is not amendable to tissues with relatively high scattering properties, e.g. brain tissue. In addition, it does not work well to recover small vessels, such as capillaries that are located beneath larger superficial vessels [17]. Indeed, for the other popular in vivo imaging subjects like human skin or mouse brain, the most of the capillaries are significantly smaller than the big superficial vessels, hence an accurate peak detection is challenging due to their relatively small signal intensities compared to tail artifacts.

Here, we propose a simple post-processing method to provide depth-resolved OCT angiography images with tail artifacts minimized, allowing accurate visualization and quantification of cortical vasculature in brain tissue. We first enhance the effective signal-to-noise ratio (SNR) in OCTA cross-sectional images, then segment the ~300 μm of OCT and OCTA data into 10 depth-layers using an automated segmentation method [18]. Finally, we utilize the enface OCT structural images from the segmented layers to create an adaptive mask that is used for suppressing the tail artifacts from enface OCTA images of the deeper cortex layers. This method is applied to OCTA images of healthy and ischemic mouse brain *in vivo* and its capability is demonstrated with several quantitative analyses. This post-processing method can also be adapted to data acquired using common OCTA systems for various applications.

2. System and methods

2.1 Animal model

All experimental animal procedures performed in this study are approved by the Institute of Animal care and Use Committee (IACUC) of the University of Washington (Protocol number: 4262-01). Male 12-week-old C57/BL6 mice weighing between 23 g to 25 g were purchased from Charles River Laboratories (Seattle, WA, USA). The mouse was deeply anesthetized using 1.5–2% isoflurane (0.2 L/min O2,

0.8 L/min air) during the experiments and euthanized at the end of the experiments. The body temperature of the animal was maintained at 36.8 C through homeothermic blanket system (507220-F, Harvard Apparatus, MA, USA). The mouse was subjected to two imaging sessions: Baseline and permanent middle cerebral artery (MCA) occlusion. An open-skull cranial window was used to increase the penetration depth of OCT signal, covering the distal branches of MCA.

Surgical procedure is briefly described as follows: First, a standard 4 × 4 mm cranial window [19] was created on the left parietal cortex 1 mm lateral from sagittal suture and 1 mm posterior from bregma by drilling a circular grooved cranium and lifting the central island. A round cover-glass was then placed over the exposed brain surface and sealed onto the bone with dental cement. Then, the cranial window was subjected to a baseline imaging by OCTA (see Section 2.3). After the baseline imaging, the mouse was subjected to a permanent coagulation of the distal MCA occlusion (dMCAO) [20]. Another set of OCTA images were taken at the same region under the cranial window right after dMCAO.

2.2 System setup

A spectral domain OCT (SD-OCT) system was used for the experiments that comprises a superluminescent diode (Thorlabs Inc., Newton, NJ, USA) as the light source [21]. This source has a central wavelength of 1,340 nm with a bandwidth of 110 nm and provides a ∼7 μm axial resolution in the air. In the sample arm, 10× scan lens (Thorlabs Inc., Newton, NJ, USA) was used to achieve ∼7 μm lateral resolution with 0.12 mm depth of field. A home-built spectrometer, which had a designed spectral resolution of ∼0.141 nm, provided a detectable depth range of ∼3 mm on each side of the zero delay line. The line rate of the linescan camera (1024 pixel detector-array, Goodrich Inc., Princeton, NJ, USA) employed in this spectrometer was 92 kHz. The system had a measured dynamic range of 105 dB with the light power of 3.5 mW incident onto the sample surface. The operations for sample beam scanning, data acquisition and storage are controlled by a custom software package written in Labview.

2.3 OCTA with increased SNR

In order to acquire OCTA images of mouse cerebral cortex, we used OCT-based microangiography (OMAG) scanning protocol [8]. In this protocol, 400 A-lines covering a distance of ∼2 mm constituted one B-frame (fast axis). In the slow axis (C-scan), there were 400 different locations equally spaced, also covering a distance of ∼2 mm. At each location, 24 repeated B-frames were acquired. With this scanning protocol, the data cube of one complete 3D scan was composed of 1024 by 400 by 9600 (z–x–y) voxels, which took ∼54 s to acquire with an imaging rate of 180 fps. The final 3D OCTA image was composed of 1024 by 400 by 400 (z–x–y) voxels.

To obtain microvasculature down to capillary level at each location, an eigenvalue decomposition (ED) based algorithm [22] was used to separate structural tissue from flowing erythrocytes from the 8 B-frames to acquire 2 types of images: The first one using an ensemble of 8 consecutive B-frames, and the second one using an ensemble of 8 B-frames obtained by skipping 2 frames in between frames out of 24 total frames. In this way, the time interval Δt for the 2nd image is three times that of the 1st image. The increase of Δt in computing OCTA results in higher sensitivity [8], but with a cost of increased noise.

Figure 1 shows the steps taken to acquire OCTA with increased SNR by combining the relatively less noisy original OCTA image with the higher sensitivity image. Briefly, after collecting 24 B-frames from one location, we applied ED algorithm to each successive 8 B-frames of 24 total B-frames to get 3 OCTA images (Step 1). Then, we compared these 3 blood flow images and picked the pixels with the maximum intensity to create an OCTA image that has a stronger signal (Step 2). In step 3, we transformed the image obtained at Step 2 into a guidance image by replacing the intensity value at each pixel with the standard deviation around that pixel (using a moving 3 × 3 kernel). Accordingly, the standard deviations of the surrounding pixels are larger at capillaries locations. In Step 4, we generated another OCTA image obtained with the ensemble of 8 B-frames with 2 frames interval out of the 24 B-frames. The frame skipping increases a time spacing between the inter B-frames, beneficial to increase OCTA signal strength at the capillaries by reducing a latency time between RBCs in single file flow at the expense of raised additive noise [8]. The pixel intensities of capillaries in original image in Step 1 were replaced with those of the image in Step 4 of which coordinates were guided by the pixel coordinates in the image in Step 3. Accordingly, if the standard deviation value in Step 3 were bigger than an empirically chosen threshold, those pixel coordinates were assigned as a capillary location. Eventually, final image (Step 5) had increased flow signal strength at the capillaries relative to the original image (Step 1) while the background stayed less noisy than the image at Step 4. This way, we effectively increased the SNR of OCTA image as shown in Step 5.

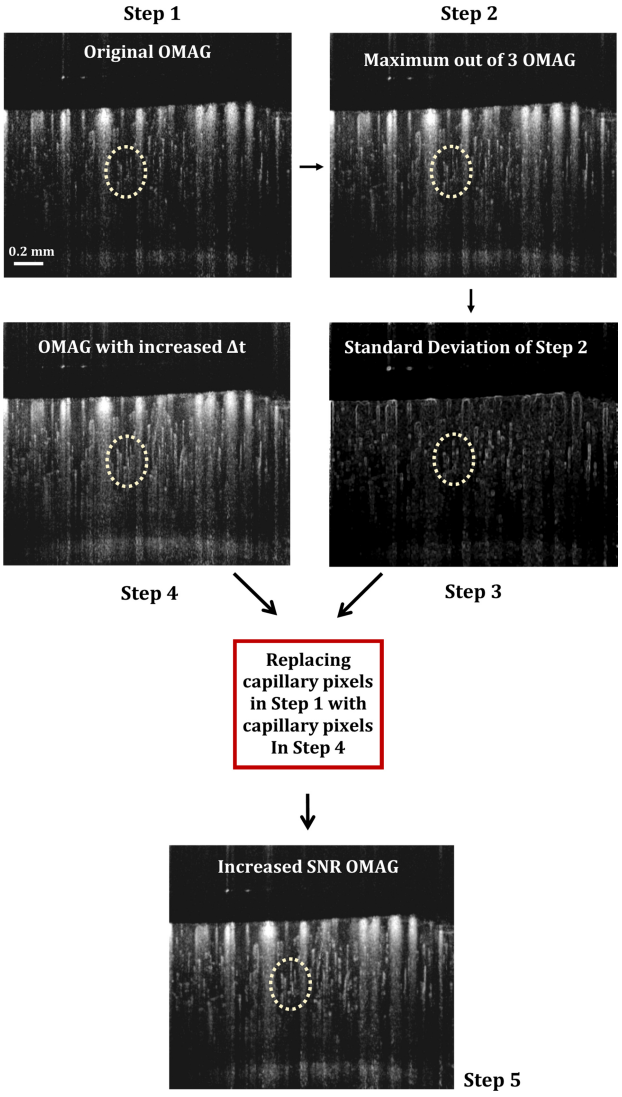

Figure 1 The sketch of steps used to generate increased SNR OCTA image. The final image in step 5 is formed by selectively combining background and big vessel pixels from step 1, and capillaries from step 4. This selective combination is done using step 3 as a guide to locate the capillaries. Accordingly, the standard deviations of the surrounding pixels (with 3×3 kernel) are larger at capillary locations as shown in step 3. This information is utilized to decide if the corresponding pixel is likely to be from a capillary, when combining images in step 1 and step 4. Dashed circles are used to highlight the improvements in SNR in capillaries.

2.4 Automated segmentation and enhancement of OCT images

In order to accurately map structure and microvasculature at various depths within cortex, we automatically segmented OCT and OCTA data. We utilized our recently developed automated segmentation and enhancement method [18] for this task. Briefly, we detected the boundary of the brain surface of in an A-line in OCT image. After this step, we selected ~300 μm within the cortex and divided it into 10 depth-layers, each with ~30 μm thickness. To acquire enface projection images from these segmented layers, we applied sorted maximum intensity projection (sMIP) algorithm [18] for each layer of every A-line where the maximum intensity of flow was selected and mapped to an enface plane. We finally applied a Gaussian filter (with 2×2 kernel) to smooth the obtained enface projection maps.

2.5 Tail artifact removal in depth-resolved OCTA images

We propose to utilize automatically segmented enface OCT structure images at deeper layers to remove the tail artifacts in depth-resolved enface OCTA images of *in vivo* mouse cortex. The enface OCT structural images at deeper layers contain a region with low intensity (shadow cast) due to the light attenuation at the superficial blood vessels which creates a contrast with the surrounding tissue. On the other hand, same regions look brighter in enface OCTA images due to the tail artifacts (caused by forward scattering of light), as shown in Figure 2A. Although, the capillaries underneath the surface vessels are difficult to detect due to a strong forward scattering event, at deeper layers, they generate comparable scattering contrast to the shadow artifacts as shown in Figure 2B. Here, we created a mask by normalizing the structural images with an adaptive threshold, and multiplied the depth-resolved enface OCTA images with the resulting mask to remove the tail artifacts while keeping some of the signal in capillaries within the tail artifacts.

The non-flat surface of the cortex makes the OCT structure image intensity non-uniform in enface cross sections. This situation is more severe when a large field of view is used. Hence, to create a structural image mask, first the enface OCT structure images at various depths were made uniform using adaptive histogram equalization [23]. Histogram equalization is a contrast enhancement technique that increases the global contrast of images when the information content is represented by close contrast values. In this work, an extension of this method, called adaptive histogram equalization, was used to enhance the foreground and suppress the noise [23]. After this step, the enface OCT structure images, $I_{\mathrm{Str}}(x,\ y,\ z)$, were normalized as below:

$$I_{\mathrm{Str\text{-}norm}}(x,\ y,\ z) = \mathrm{Normalize}\ (I_{\mathrm{Str}}(x,\ y,\ z),\ \mathrm{low}\,(z),\ \mathrm{high}\,(z)) \quad (1)$$

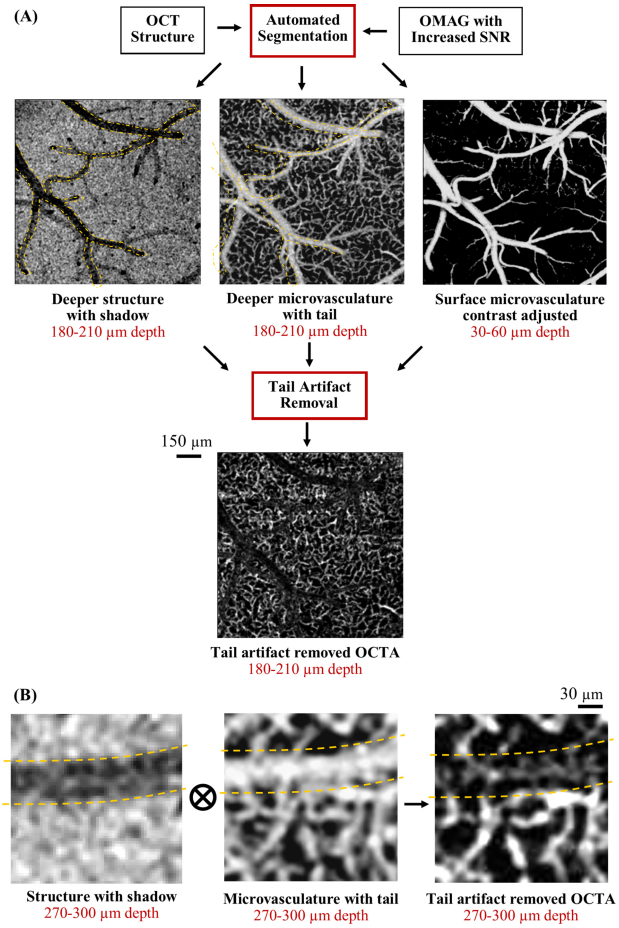

Figure 2 Overall procedure of acquiring tail artifact removed depth-resolved enface OCTA images of rodent cortex. (**A**) After automated generation of depth-resolved enface OCT structure and OMAG images, tail artifact algorithm removes the tailing artifacts at deeper layers while keeping some of the capillary plexus intact. (**B**) Magnified images of structure with shadow cast, microvasculature with tail artifact and the final tail artifact suppressed OCTA image that is obtained by multiplying the enface microvascular image with the mask created by normalizing the enface structural image with adaptive threshold. Yellow dashed lines point out the artifact locations.

Here, $\mathrm{low}\,(z)$ and $\mathrm{high}\,(z)$ refer to the contrast thresholds for different layers, z, where $z = \{1, 2, \ldots, 10\}$. These thresholds were adaptively chosen as the mean and maximum intensity values of depth-resolved enface OCT structure images, $I_{\mathrm{Str}}(x, y, z)$, respectively.

To remove the tails of big surface vessels more effective in the deeper layers, we subtracted the contrast-adjusted enface OCTA image of the second layer ($z = 2$) from the deeper layers with a scaling factor, $0 < \alpha(z) < 1$. Finally, we multiplied the depth-resolved enface OCTA images from layers (z) 4 to 10 with the adaptive structure masks we created in the previous step as below:

$$I_{\text{Flow-out}}(x, y, z) = [I_{\text{Flow}}(x, y, z) - I_{\text{Flow}}(x, y, 2) \times \alpha(z)] \times I_{\text{Str-norm}}(x, y, z) \quad (2)$$

where $I_{\text{Flow-out}}(x, y, z)$ represents the output pixel intensity of an enface OCTA image in the layer z, and $I_{\text{Flow}}(x, y, z)$ refers to the original enface OCTA pixel intensity at layer z. It is important to note that the choice of $\alpha(z)$ is dependent on the layer depth; it was chosen larger for the layers 4 and layer 5 to remove the strong tail artifacts and smaller for the deeper layers where the OCT structure mask becomes more effective to remove the tail artifacts and enhance signal contrast at capillaries. The exact value of $\alpha(z)$ depends on the system configuration, and the tissue optical property as well as its physiology.

3. Results

3.1 Depth-resolved OCTA within healthy and ischemic mouse cerebral cortex

Cerebral microvasculature in mouse was imaged through an open-skull cranial window using OCT. The vessel densities in cortex changes with different cortical layers, so it is important to reveal true vessel density distribution for a better understanding of neurovascular coupling during normal and diseased conditions. The top panel in Figure 3 shows the depth-resolved enface OCTA images of healthy mouse cortex in vivo before applying the proposed method and compares with the results from the proposed method at the right panel. At the depth of 90–120 μm under the surface, a bigger scaling factor α was necessary to remove the tail artifacts, but in return it also suppressed the capillaries in these tails artifacts. Starting from ~150 μm depth, capillaries could be visualized within the tail artifacts after the removal procedure. Due to the contrast adjustment effect of adaptive enface OCT structure masks, the capillaries also appear brighter in the depth-resolved enface OCTA images.

Moreover, Figure 4 shows the original depth-resolved enface OCTA images of ischemic mouse cortex *in vivo* and compares with the results from the proposed method. Procedure of dMCAO created a large ischemic region which can be seen in the images shown. Although the arteriolo-arteriolar anastomosis recovered some of the missing blood in MCA through stealing blood from the collateral network, the majority of the MCA vicinity still remained ischemic [21]. As shown in Figure 4, in the original OCTA images, the tail artifacts coming from MCA appear in the deeper layers of ischemic corti-

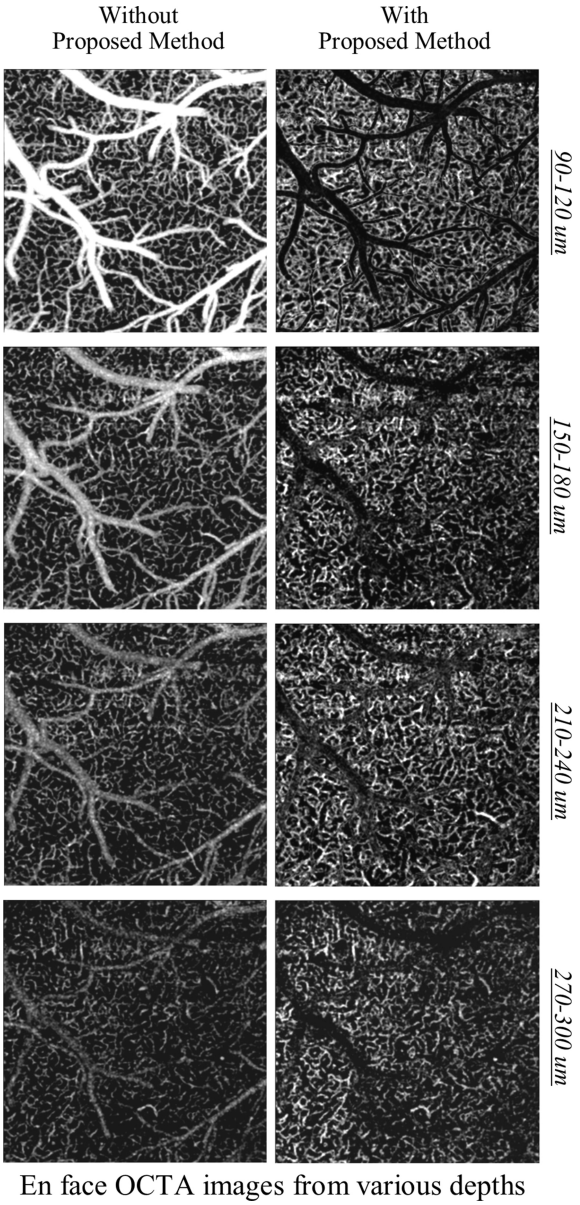

Figure 3 Comparison between original depth-resolved en-face OCTA images of healthy mouse cortex *in vivo* with the results from the proposed method. The open-skull cranial window was used. The field of view in the images is 1.5 mm × 1.5 mm.

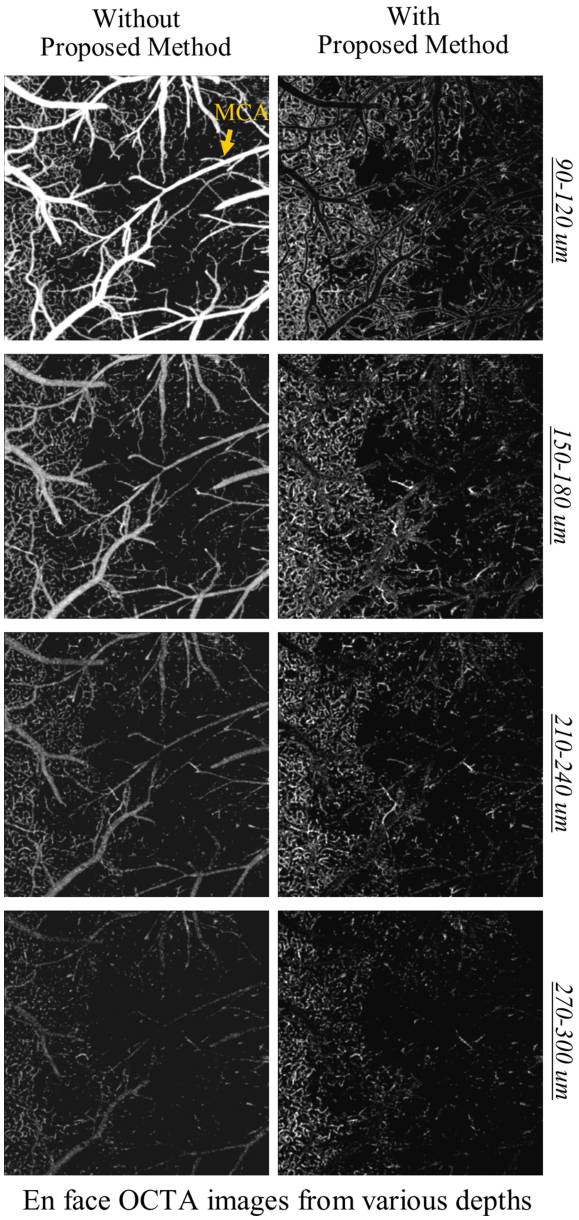

Figure 4 Comparison between original depth-resolved en-face OCTA images of ischemic mouse cortex *in vivo* with the results from the proposed method. The open-skull cranial window was used. Ischemic region is formed after dMCAO. Occluded MCA branch is pointed out. The field of view in the images is 2 mm × 2 mm.

cal area, which can lead to an inaccurate quantification. Using the proposed method, capillary dropout in that region can be easily distinguished.

3.2 Comparison of vessel area density and vascular dissimilarity in depth-resolved enface OCTA images

To quantify the tail artifact removal effect on depth-resolved angiograms, we calculated the vessel area densities (VADs) of angiograms at each layer (L1–L10). The VAD is calculated as a ratio of a number of pixels covered by the vessels to the total number of pixels in the image [24]. Figure 5A and B show comparison of the calculated VADs with/without tail artifact removal for healthy and ischemic mice, respectively. For healthy one, the VAD started to decrease from L3. The decrease in the VAD might be due to either cortical vessel geometry or attenuation

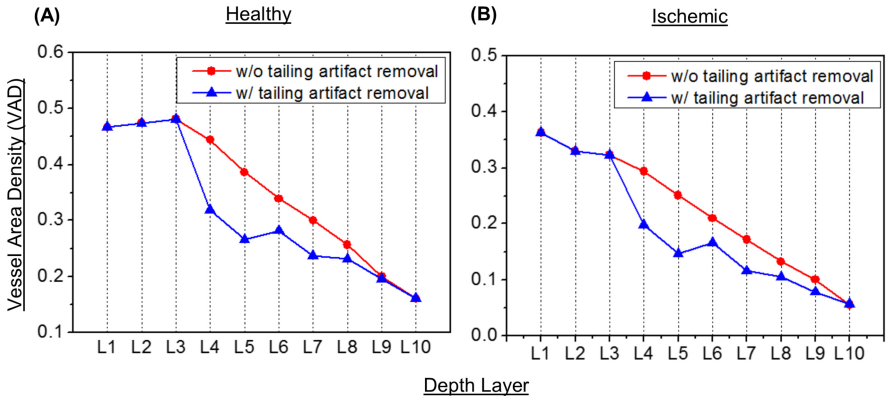

Figure 5 Comparison of cortical vessel area density (VAD) as a function of depth calculated from OCT angiograms of (**A**) healthy and (**B**) ischemic mice. The open-skull cranial window was used. Ischemic region was formed after dMCAO.

of OCTA signal strength in depth. With the tail artifact removal, however, the VAD quickly dropped at L4. This is because of the complete removal of tail artifacts of superficial vessels from L4 and L5 without being able to distinguish capillaries underneath at these tails (see Figures 3–4, 90–120 μm depth images). Starting from L6, the capillaries in these tails were partially preserved after the tail artifact removal (see Figures 3–4, 150–300 μm depth). In contrast, without the tail artifact removal, the VADs remained relatively high, due to the presence of strong tails in the enface OCTA images that deceive the VAD calculation algorithm. This trend was similar in the ischemic case as shown in Figure 5B.

Moreover, the local geometry of microvasculature in the superficial cortical vessel network is quite different from the vascular networks below the surface that consists of many capillaries [1]. We compared dissimilarity between the enface OCTA images by calculating correlations between the image at the surface (L3) and four others below the surface (L4, L6, L8, and L10). The results were graphically represented for healthy and ischemic mice in Figure 6A and B, respectively. After the tail artifact removal, all the sub-surface angiograms at L4, L6, L8, and L10 were highly uncorrelated with the surface angiogram at L3. On the other hand, with no tailing artifact removal, the correlation value between angiograms (L3 and L4) was close to 1 (totally correlated) and more than 0.3 at even much deeper layer (L10). It indicates that the artificial flow signals from the surface vessels appearing at the deeper layers increase the vascular similarity in vessel geometry, resulting in substantial error for vessel visualization and quantification. Similar trend was also found for the ischemic mouse cortex as shown in Figure 6b, but its correlation values were slightly higher than the healthy case (Figure 6A). This can be explained by the capillary dropout observed in MCA side after dMCAO which makes images more similar in comparison (see Figure 4).

4. Discussion and conclusion

Within the interconnected network of microvasculature in brain, penetrating vessels that are directly attached to the surface pial arterioles branch as a function of depth, resulting in a broad variation in the density of microvasculature at different cortex layer [1]. The distribution of vessel density is strictly regulated at different cortical layers, corresponding to a function of depths of neuronal cells. Moreover, pathological, physiological, and environmental states can influence or promote changes in capillary density. For example, chronic hypoxia increases capillary density [25]. This adaptive increase in capillary

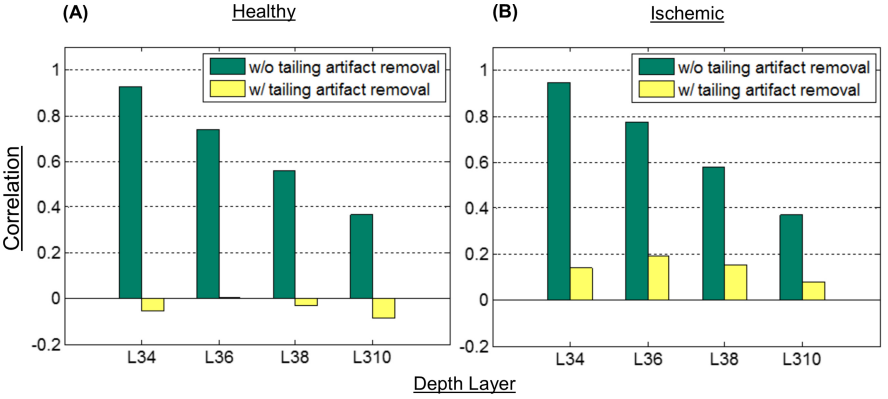

Figure 6 Comparison of correlation values between enface angiogram at L3 and each enface angiograms at L4, L6, L8, and L10 for (**A**) healthy and (**B**) ischemic mice, respectively. The open-skull cranial window was used. Ischemic region was formed after dMCAO.

density during chronic hypoxia increases cerebral blood volume and restores tissue oxygen tension. Hypertension also affects brain capillary density by causing rarefaction (decrease in number) of capillaries and impaired microvessel formation that can increase vascular resistance [26]. An accurate quantification of microvasculature in deeper brain layers (capillary layer) is essential to understand cerebral vascular condition in heathy and diseased states.

In this work, we proposed to utilize enface depth-resolved OCT structural images to remove the tail artifacts in enface OCTA images acquired from the deeper layers of mouse cerebral cortex, *in vivo*. The proposed algorithm is shown useful in suppressing tail artifacts present in enface OCTA images, leading to improved visualization of the deeper microvascular plexus under the big surface vessels, which are originally not visible due to these artifacts. Thus, the continuity of deeper vascular networks is preserved for the benefit of qualitative and quantitative studies.

The proposed method assumes that the capillaries at deeper layers generate a comparable scattering contrast to the shadow casts in enface OCT structure images. This assumption is not strictly true when they are right underneath the big vessels (~90–150 μm under the surface) where the forward scattering event is still strong. Therefore, for these areas (layers 4 and 5 in our segmented volume) we subtracted surface vessels using a larger ratio, α, to eliminate the tail artifacts (see Eq. (2)). However, the information of capillary plexus beneath the big surface vessels up to ~150 μm was also lost during this operation (Figures 3–4). Another important assumption of this method is that the scattering contrast inside the shadows of enface OCT structure images at the deeper layers (Figure 2B) come from the flowing erythrocytes in capillaries. This assumption is based on the fact that the high scattering regions inside these shadows are aligned well with the surrounding microvasculature and are non-uniformly distributed. Moreover, these tail artifacts mostly appear under the big surface vessels and have a larger footprint than the capillaries in the deeper layers, which make their removal easily distinguished compared to the effect of this algorithm on capillary plexus (Figures 3–4).

We utilized this method in a stroke study on mouse for quantifying vessel density changes after dMCAO, in vivo. Figure 5 demonstrates that the tail artifacts lead to an increase in the calculated VADs in the depth-resolved enface OCTA images of healthy and ischemic mouse brain in vivo, which make these results difficult to interpret for comparison studies. The ability of seeing through the tails of surface vessels enabled more accurate capillary density calculations in deeper layers of cerebral cortex. Moreover, we quantified the dissimilarity between the enface OCTA images by calculating correlations between the image at the surface and four others below the surface. As expected, the vessel morphology in the images acquired after the application of the proposed method are highly dissimilar to the surface vessel morphology, whereas the tail artifacts lead to large correlation values between them (see Figure 6).

4.1 Limitations

OCTA offers a unique ability to quickly image a relatively large area in time-sensitive stroke experiments. However, it comes with some limitations. Firstly, the lateral resolution of our system is ~7 μm with a depth of focus of 0.12 mm. The limited resolution makes it difficult to resolve capillaries that are closely positioned to each other and can lead to inaccuracies in VAD calculations. On the other hand, the areas outside of the depth of focus appear blurred in the enface images and can also lead to inaccurate VAD calculations. In this study, we tried our best to keep all the crucial parameters, such as the focus of the probe beam, positioning and orientation of the sample to be the same among all the imaging sessions.

The proposed algorithm is simple and yet effective to remove the tail artifacts in deeper layers, however it is not perfect. Especially the problem of differentiating capillaries that are closer to the big surface vessels (up to ~150 μm) remains as a significant challenge. Alternative hardware-based method, dynamically focused optical coherence microscopy (OCM) angiography with a high numerical aperture, has shown to be successful at reducing the tail artifacts in synthesized angiograms [27]. Moreover, the multiplication of enface structural images with angiography images might also suppress the signal in some of the capillaries that are not underneath a big blood vessel as seen in Figure 2B. However, this side effect is relatively weak, thanks to the SNR increase in capillaries before the application of our method (see Section 2.3). Future work will also focus on translating this method into a volumetric visualization of tail artifact removed OCTA.

In summary, the strongly forward scattering of photons propagating within the blood vessels causes variations in OCT signals, leading to tail artifacts in OCTA images beneath the functional blood vessels. In spite of the availability of various algorithms, it is still difficult to exclude these artifacts in the OCTA images while preserving the capillaries inside these tails. Here, we have shown that using our simple method we can remove these artifacts while keeping some of the small vessels underneath intact in enface OCTA images for rodent brain imaging applications.

Due to its post-processing implementation, it can be easily used in the standard OCT systems. In this study, we focused on a stroke model in mice to show the usefulness of this method but it is reasonable to believe that this post-processing method can be adapted for various other applications.

Acknowledgements The work was supported in part by National Institutes of Health grants (R01HL093140, and R01EB009682).

References

[1] B. Pablo, P. S. Tsai, J. P. Kaufhold, P. M. Knutsen, H. Suhl, and D. Kleinfeld. Nat. Neurosci **16**(7), 889–897 (2013).
[2] D. A. Boas and A. K. Dunn. J. Biomed. Opt. **15**(1), 011109 (2010).
[3] C. K. Willie, F. L. Colino, D. M. Bailey, Y. C. Tzeng, G. Binsted, L. W. Jones, M. J. Haykowsky, J. Bellapart, S. Ogoh, K. J. Smith, J. D. Smirl, T. A. Day, S. J. Lucas, L. K. Eller, and P. N. Ainslie. J. Neurosci. Methods **196**(2), 221–237 (2011).
[4] D. P. Cardenas, E. R. Muir, S. Huang, A. Boley, D. Lodge, and T. Q. Duong. NeuroImage **119**, 382–389 (2015).
[5] C. Schaffer, B. Friedman, N. Nishimura, L. Schroeder, P. Tsai, F. Ebner, P. Lyden, and D. Kleinfeld. PLoS Biol. **4**(2), e22 (2006).
[6] P. H. Tomlins and R. K. Wang. J. Phys. D: Appl. Phys. **38**(15), 2519–2535 (2005).
[7] R. K. Wang, S. L. Jacques, Z. Ma, S. Hurst, S. R. Hanson, and A. Gruber. Opt. Express **15**(7), 4083–4097 (2007).
[8] L. An, J. Qin, and R. K. Wang. Opt. Express **18**(8), 8220–8228 (2010).
[9] H. Wang, U. Baran, Y. Li, W. Qin, W. Wang, H. Zeng, and R. K. Wang. J. Biomed. Opt. **19**(10), 106011 (2014).
[10] L. Themstrup, J. Welzel, S. Ciardo, R. Kaestle, M. Ulrich, J. Holmes, R. Whitehead, E. C. Sattler, N. Kindermann, G. Pellacani, and G. B. E. Jemec. Microvasc. Res. **107** (2016).
[11] U. Baran, W. J. Choi, and R. K. Wang. Skin Res Technol **22**(2), 238–246 (2015).
[12] Q. Q. Zhang, C. S. Lee, J. Chao, C.-L. Chen, T. Zhang, U. Sharma, A. Zhang, J. Liu, K. Rezaei, K. L. Pepple, and R. Munsen. Scientific reports **6** (2016).
[13] U. Baran and R. K. Wang. Neurophotonics **3**(1), 010902 (2016).
[14] V. J. Srinivasan and H. Radhakrishnan. NeuroImage **102**, 393–406 (2014).
[15] L. Liu, S. S. Gao, S. T. Bailey, D. Huang, D. Li, and Y. Jia. Biomed. Opt. Express **6**(9), 3564–3576 (2015).
[16] A. Zhang, Q. Zhang, and R. K. Wang. Biomed. Opt. Express **6**(10), 4130–4143 (2015).
[17] M. Zhang, T. S. Hwang, J. P. Campbell, S. T. Bailey, D. J. Wilson, D. Huang, and Y. Jia. Biomed. Opt. Express **7**(3), 816–828 (2016).
[18] U. Baran, W. Zhu, W. J. Choi, M. Omori, W. Zhang, N. J. Alkayed, and R. K. Wang. J Neurosci. Methods **270**(1), 132–137 (2016).
[19] Y. Li, U. Baran, and R. K. Wang. PLoS ONE **9**(11), e113658 (2014).
[20] G. Llovera, S. Roth, N. Plesnila, R. Veltkamp, and A. Liesz. JoVE **89**, e51729 (2014).
[21] U. Baran, Y. Li, and R. K. Wang. Neurophotonics **2** (2), 025006 (2015).
[22] S. Yousefi, Z. Zhi, and R. K. Wang. IEEE T Biomed Eng. **58**(8), 2316–2323 (2011).
[23] Y. Siavash, J. Qin, Z. Zhi, and R. K. Wang. Quant. Imaging Med. Surg. **3**(1), 5–17 (2013).
[24] R. Reif, J. Qin, L. An, Z. Zhi, S. Dziennis, and R. K. Wang. J. Biomed. Opt. **2012**, 9 (2012).
[25] M. J. Cipolla. The Cerebral Circulation. San Rafael (CA): Morgan & Claypool Life Sciences; Chapter 2, Anatomy and Ultrastructure. (2009).
[26] I. A. Sokolova, E. B. Manukhina, S. M. Blinkov, V. B. Koshelev, V. G. Pinelis, and I. M. Rodionov. Microvasc. Res. **30**(1), 1–9 (1985).
[27] L. Conor, H. Radhakrishnan, M. Bernucci, and V. J. Srinivasan. J. Biomed. Opt. **21**(2), 020502 (2016).